Progress In Electromagnetics Research B, Vol. 32, 299–317, 2011

COMPARATIVE STUDY OF FABRY-PEROT RESONATOR ANTENNA WITH PMC AND PEC GROUND PLANE

Z.-G. Liu[1, *] and T.-H. Liu[2]

[1]State Key Laboratory of Millimeter Waves, Southeast University, Nanjing, China

[2]ZhongBo Information Technology Research Institute Co., Ltd., Nanjing, China

Abstract—In this paper, the transverse equivalent network (TEN) model based on the transmission line theory is employed to analyze and calculate the far-field radiation properties of the Fabry-Perot Resonator (FPR) antenna with perfect magnetic conductor (PMC) ground plane in detail, then the comparative study of the radiation property of FPR antenna with PMC and PEC ground plane is presented. The closed-form expressions for the radiated fields, field peak values, pattern beamwidths and pattern bandwidth of this type of antenna in the E- and H-planes are derived, respectively. The results demonstrate that in theory the radiation property of FPR antenna with two kinds of ground plane is not the same unexpectedly. An interesting characteristic of this type of antenna is that when the PMC acts as the antenna ground plane, the beamwidth and bandwidth of the antenna is increased by a factor of two in general cases, while its peak value of far field is the same as that of the conventional antennas of this class having PEC ground plane. Some results are validated through full-wave simulations of an actual antenna. The original results obtained here lead to a design method for getting the maximum directivity and keeping the bandwidth of this kind of resonant antenna, which is of great significance for antenna designing.

Received 23 April 2011, Accepted 5 July 2011, Scheduled 21 July 2011

* Corresponding author: Zhen-Guo Liu (liuzhenguo@seu.edu.cn).

1. INTRODUCTION

Fabry-Perot Resonator (FPR) antenna generally consists of a primary radiator backed with a metal ground plane and a partially reflective covered plate [1]. It essentially provides the benefit of high directivity without requiring the complex network, as the conventional antenna arrays. It has aroused more and more attention [2–4] for several years, which results in some interesting conclusions based on different viewpoints and analysis models such as leaky wave model [5–10], EBG defect model [11–16], FP cavity model [1, 2, 17, 18], equivalent refractive lens model [19, 20] have been attained and proposed. A summary of this type of antenna is also presented in [19, 21].

In addition, artificial magnetic conductor (AMC) [22–24] has also been proposed to act as ground plane of FPR antenna to improve its performance such as reducing resonant cavity profile [3, 4, 15, 25–27] due to its property to fully reflect incident waves with approximate zero phase shift. It is referred to as a perfect magnetic conductor (PMC), which is complementary to a perfect electric conductor (PEC). But to our knowledge, other far field radiation properties such as radiated fields, field peak values, pattern beamwidths, etc. have not been studied in detail. In this paper, the general expressions are obtained firstly for radiation properties of FPR antenna with PMC ground plane by using simple TEN model [9–10, 27] based on reciprocity theory and transmission line theory. This provides design guidelines and a physical insight into the function of PMCs. In addition, the comparison results of radiation properties between FPR antenna with PMC and with PEC ground plane are also performed in detail, and some part of which have been present in [28].

2. ANALYSIS AND DESIGN

2.1. TEN Model

The transverse equivalent network (TEN) model is a simple method for evaluating the far field radiation properties of resonator antennas such as the directivity and radiation patterns [9]. Its accuracy has also been compared with the numerically exact results obtained from the method such as MoM in [9]. It also provides an excellent agreement with other complicated methods based on Green's function calculations in [5] or leaky-wave analysis in [6, 7]. The biggest advantage of the TEN model is its extreme simplicity compared with those of the full-wave analyzers, while giving the peak directivity and resonant conditions with adequate accuracy.

Figure 1(a) shows the geometry of the proposed FPR antenna. The resonant cavity is composed of a completely reflecting surface PMC or PEC, a partially reflective surface (PRS) and a dielectric substrate with permittivity ε_{r1} (ε_{r1} can also be equal to 1, which means air substrate). They are all assumed to be infinite in the transverse direction. The distance between two parallel planes is D. An x-directional primary dipole source is placed at a distance h from the ground plane. The PRS is assumed to be a homogeneous surface in the analysis.

According to reciprocity theory, the calculation of the far-field can be reduced to a plane-wave excitation on the structure. This is done by placing a testing dipole in the far field ($kr \gg 1$) at the observation point, in $\hat{\theta}$ or $\hat{\varphi}$ direction. The far field E_θ or E_φ at (r, θ, φ) due to a source dipole at $z = h$ is by reciprocity the same as E_x at $z = h$ due to testing dipole at (r, θ, φ) in $\hat{\theta}$ or $\hat{\varphi}$ direction, which may be taken as a plane wave due to the far-field location of the testing dipole. Hence, reciprocity indicates that the electric field at $z = h$ due to an incident plane wave is proportional to far field radiated by a source electric dipole at $z = h$. Therefore, the TEN model can be used for calculating the radiation pattern of such a kind of antenna, which is applicable to any general class of that consists of a PMC or PEC grounded slab covered with a PRS and excited by a simple source. Using the TEN model, this antenna is simplified to the structure consisting of sections of transmission lines terminated by a load. The transmission line analogy for PMC and PEC ground is shown in Fig. 1(b) and Fig. 1(c), respectively. In this model, a shunt admittance is used to represent the PRS.

For the E_φ component, the corresponding incident wave is vertically polarized with the incident voltage V_{inc}^{TE}, given by [9]:

$$V_{inc}^{TE} = -E_0 \sin\varphi = (j\omega\mu_0/4\pi r)e^{-jk_0 r}\sin\varphi. \tag{1}$$

For the E_θ component, on the other hand, the incident wave is of horizontal polarization with the incident voltage V_{inc}^{TM} expressed as [9]:

$$V_{inc}^{TM} = E_0 \cos\theta\cos\varphi = (-j\omega\mu_0/4\pi r)e^{-jk_0 r}\cos\theta\cos\varphi, \tag{2}$$

where E_0 represents the magnitude of incident field with either unit vector $\hat{\theta}$ or $\hat{\varphi}$ for TM_z or TE_z incidence.

2.2. Radiation Properties of Antenna with PMC Ground

When the ground plane is PMC in Fig. 1(b), the load impedance in the transmission line model is imaginary infinity. In [4], it is indicated that the disparities among reflection phases of PRS corresponding to

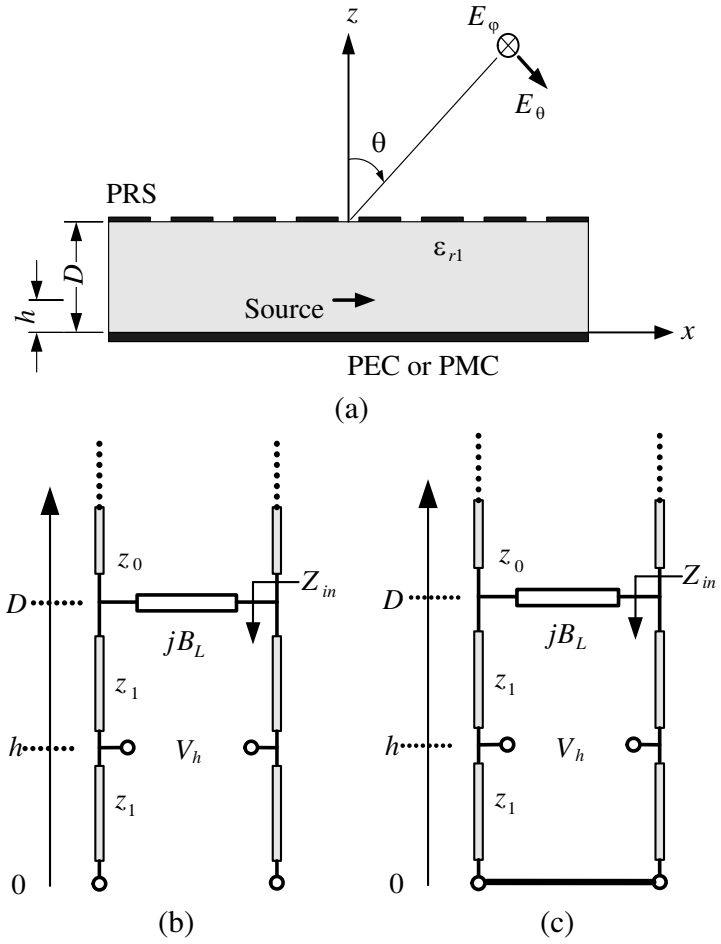

Figure 1. Fabry-Perot resonator antenna with PMC or PEC ground plane. (a) Geometry. (b) Transmission line model for PMC. (c) For PEC ground plane.

different oblique incident angles up to $\pm 60^\circ$ range are small enough to be ignored. Therefore, although PRS shunt susceptance varies with the angle of radiation, for narrow-beam regions of interest, it may be assumed to be constant. Assuming no transmission losses for PRS, thus we can express PRS shunt susceptance by $Y_L = jB_L$. According to the transmission line theory, the voltage V_h at $z = h$ is derived as

following:

$$\begin{aligned} V_{(z=h)} &= V_{(z=D)} \cos k_{z1}(D-h) - jZ_1 I \sin k_{z1}(D-h) \\ &= E_0 \frac{Y_0 \cos k_{z1} h}{Y_0 \cos k_{z1} D + j(B_L \cos k_{z1} D + Y_1 \sin k_{z1} D)} \end{aligned} \tag{3}$$

and the current I is expressed as

$$I = \frac{V_{(z=D)}}{-jZ_1 \cot k_{z1} D}, \tag{4}$$

where the admittances Y_0 and Y_1 for TE and TM polarizations have the following expressions in terms of the vertical wave numbers k_{z0} and k_{z1} in the air and slab regions, respectively

$$Y_0^{TM} = \frac{k_0}{k_{z0}\eta_0} = \frac{\sec\theta}{\eta_0}, \quad Y_0^{TE} = \frac{k_{z0}}{k_0\eta_0} = \frac{\cos\theta}{\eta_0};$$

$$Y_1^{TM} = \frac{k_0\varepsilon_{r1}}{k_{z1}\eta_0} = \frac{\varepsilon_{r1}}{\eta_0\sqrt{n_1^2 - \sin^2\theta}}, \quad Y_1^{TE} = \frac{k_{z1}}{k_0\eta_0} = \frac{\sqrt{n_1^2 - \sin^2\theta}}{\eta_0},$$

where η_0 is the free-space characteristic impedance, and n_1 is index of refraction in the dielectric slab with $n_1^2 = \varepsilon_{r1}$.

2.2.1. Far-Field Pattern in H- and E-Planes

H-Plane ($\varphi = 90^\circ$): Simplify the formula (3), and replace the admittances Y_0 and Y_1 with corresponding Y_0^{TE} and Y_1^{TE}. So the far field E_φ component is

$$E_\varphi = E_0 \frac{\cos k_{z1} h \ \sec k_{z1} D}{1 + j(\bar{B}_L + \bar{Y}_1^{TE} \tan k_{z1} D) \sec\theta}, \tag{5}$$

where the symbol "-" indicates normalization with respect to η_0, $\bar{Y}_1^{TE} = \eta_0 Y_1^{TE} = \sqrt{n_1^2 - \sin^2\theta}$, $\bar{B}_L = \eta_0 B_L$. Because the resonant condition of

$$k_{z1} D = k_0 D\sqrt{n_1^2 - \sin^2\theta} \simeq \pi/2 \tag{6}$$

is met near the peak of beam when PMC acts as ground plane, the far field may be approximated as

$$E_\varphi \simeq E_0 \frac{\cos k_{z1} h \sec k_{z1} D}{1 + j(\bar{B}_L + \bar{Y}_1^{TE} \sec k_{z1} D) \sec\theta}. \tag{7}$$

E-Plane ($\varphi = 0^\circ$): Similarly, in formula (3), replacing the admittances Y_0 and Y_1 with corresponding Y_0^{TM} and Y_1^{TM}, the far

field E_θ component can be simplified as:

$$E_\theta \simeq E_0 \cos\theta \frac{\cos k_{z1} h \sec k_{z1} D}{1 + j(\bar{B}_L + \bar{Y}_1^{TM} \sec k_{z1} D) \cos\theta}, \tag{8}$$

where $\bar{Y}_1^{TM} = \eta_0 Y_1^{TM} = \frac{\varepsilon_{r1}}{\sqrt{n_1^2 - \sin^2\theta}}$.

2.2.2. Maximum in H- and E-planes

H-Plane: In order to obtain the maximum of far field E_φ and E_θ components, respectively, the first item of the numerator in formulas (7) and (8) should be equal to 1, then $k_{z1}h = 0$. It means that for PMC ground plane case the primary source should be located directly on its surface. On the other hand, the term $(\cos k_{z1} D \cos\theta)^2 + (\bar{B}_L \cos k_{z1} D + \bar{Y}_1^{TE})^2$ should be in the minimum, then let its derivative function with respect to $\cos(k_{z1}D)$ equal to zero, and the solution of $\cos(k_{z1}D)$ is

$$\cos(k_{z1} D) = -\bar{B}_L \bar{Y}_1^{TE} / (\cos^2\theta + \bar{B}_L^2) \simeq -\bar{Y}_1^{TE} / \bar{B}_L \tag{9}$$

Hence, the maximum of E_φ is

$$E_{\varphi|\max} \simeq E_0 \frac{1}{\cos k_{z1} D} \simeq E_0 \frac{-\bar{B}_L}{\bar{Y}_1^{TE}} = E_0 \frac{-\bar{B}_L}{\sqrt{n_1^2 - \sin^2\theta}}. \tag{10}$$

At the broadside, the maximum can be expressed as

$$E_{\varphi|\max}^{broadside} = E_0(-\bar{B}_L / n_1). \tag{11}$$

E-Plane: Similarly, let $\cos(k_{z1}D) = -\bar{B}_L \bar{Y}_1^{TM} / (\sin^2\theta + \bar{B}_L^2) \simeq -\bar{Y}_1^{TM} / \bar{B}_L$, the maximum field of E_θ component is obtained as:

$$\begin{aligned} E_{\theta|\max} &\simeq E_0 \cos\theta \frac{1}{\cos k_{z1} D} \simeq E_0 \cos\theta \frac{-\bar{B}_L}{\bar{Y}_1^{TM}} \\ &= E_0 \cos\theta \frac{-\bar{B}_L \sqrt{n_1^2 - \sin^2\theta}}{\varepsilon_{r1}}. \end{aligned} \tag{12}$$

At broadside, due to $n_1^2 = \varepsilon_{r1}$, the maximum can be expressed as (10).

2.2.3. Pattern Beamwidth

H-Plane: The pattern beamwidth can be calculated by determining the angle at which the radiated power density is one half of its value

at broadside. Applying a Taylor expansion to (5) and (7) at near broadside,

$$\sec k_{z1}D \simeq \sec\left(k_0D\sqrt{n_1^2-\sin^2\theta_0}\right)+\Delta\theta\sec'\left(k_0D\sqrt{n_1^2-\sin^2\theta}\right)|_{\theta=\theta_0} + \frac{1}{2}(\Delta\theta)^2\sec''\left(k_0D\sqrt{n_1^2-\sin^2\theta}\right)|_{\theta=\theta_0} \quad (13)$$

where $\theta_0 = 0$. Substituting it into formula (5), the E_φ expression is

$$E_\varphi \simeq E_0 \frac{\sec\left(k_0D\sqrt{n_1^2-\sin^2\theta_0}\right)+\frac{1}{2}(\Delta\theta)^2\sec^2\left(k_0D\sqrt{n_1^2-\sin^2\theta_0}\right)\left(\frac{-k_0D}{n_1}\right)}{\left(\begin{array}{l}1+j\left[\bar{B}_L+\bar{Y}_1^{TE}\left(\sec\left(k_0D\sqrt{n_1^2-\sin^2\theta_0}\right)\right.\right.\\ \left.\left.+\frac{1}{2}(\Delta\theta)^2\sec^2\left(k_0D\sqrt{n_1^2-\sin^2\theta_0}\right)\left(\frac{-k_0D}{n_1}\right)\right)\right]\sec\theta\end{array}\right)} \quad (14)$$

At the peak, the resonance condition $\bar{B}_L+\bar{Y}_1^{TE}\sec k_0D\sqrt{n_1^2-\sin^2\theta_0}=0$ is satisfied. So formula (14) can be simplified as

$$E_\varphi \simeq E_0\frac{\left(-\frac{\bar{B}_L}{\bar{Y}_1^{TE}}\right)}{1+j\frac{1}{2}(\Delta\theta)^2\left(-\frac{\bar{B}_L}{\bar{Y}_1^{TE}}\right)^2\left(\frac{-k_0D}{n_1}\right)}. \quad (15)$$

At the angle of $\Delta\theta$, the absolute of the imaginary and real parts of the denominator of (15) are equal, so $|\frac{1}{2}(\Delta\theta)^2(-\frac{\bar{B}_L}{\bar{Y}_1^{TE}})^2(\frac{-k_0D}{n_1})|=1$. The pattern beamwidth at broadside is

$$\theta_{3\,\mathrm{dB}} = 2\Delta\theta = 2\sqrt{\frac{4n_1^3}{\bar{B}_L^2\pi}}. \quad (16)$$

For general case (when the maximum of radiation field is not in broadside), the Taylor expansion to (6) is written as

$$\sec k_{z1}D \simeq \sec\left(k_0D\sqrt{n_1^2-\sin^2\theta_0}\right)+\Delta\theta\sec'\left(k_0D\sqrt{n_1^2-\sin^2\theta}\right)|_{\theta=\theta_0}, \quad (17)$$

where $\theta_0 \neq 0$. Substituting it into the formula (5), then the E_φ expression is given as

$$E_\varphi \simeq E_0 \frac{\begin{pmatrix} \sec\left(k_0 D\sqrt{n_1^2-\sin^2\theta_0}\right) \\ +\Delta\theta \sec^2\left(k_0 D\sqrt{n_1^2-\sin^2\theta_0}\right)\left(\frac{-k_0 D\sin\theta_0\cos\theta_0}{\sqrt{n_1^2-\sin^2\theta_0}}\right) \end{pmatrix}}{\begin{pmatrix} 1+j\left[\bar{B}_L+\bar{Y}_1^{TE}\left[\sec(k_0 D\sqrt{n_1^2-\sin^2\theta_0}) \right.\right. \\ \left.\left. +\Delta\theta \sec^2\left(k_0 D\sqrt{n_1^2-\sin^2\theta_0}\right)\left(\frac{-k_0 D\sin\theta_0\cos\theta_0}{\sqrt{n_1^2-\sin^2\theta_0}}\right)\right]\right]\sec\theta \end{pmatrix}} \quad (18)$$

The pattern beamwidth for general cases is obtained from

$$\Delta\theta \cdot \bar{Y}_1^{TE}\sec^2\left(k_0 D\sqrt{n_1^2-\sin^2\theta_0}\right)\left(\frac{k_0 D\sin\theta_0}{\sqrt{n_1^2-\sin^2\theta_0}}\right) = 1. \quad (19)$$

Hence, the result is

$$\theta_{3\,\mathrm{dB}} = 2\Delta\theta = \frac{4(n_1^2-\sin^2\theta)^{3/2}}{\overline{B}_L^2 \pi \sin\theta}. \quad (20)$$

E-Plane: From (8), performing the similar analysis process the explicit expressions of beamwidth in E-plane can be derived as shown in Table 1.

2.2.4. Pattern Bandwidth

H-Plane: The antenna bandwidth for radiation is defined as the frequency range where the level of power density radiated is 3 dB lower than its maximum. Applying a Taylor expansion to (7) and (8) with regard to f respectively,

$$\sec k_{z1}D = \sec\left(\frac{2\pi f_0 D}{c}\sqrt{n_1^2-\sin^2\theta_0}\right) \simeq \sec\left(\frac{2\pi f_0 D}{c}\sqrt{n_1^2-\sin^2\theta_0}\right) + \Delta f \sec^2\left(\frac{2\pi f_0 D}{c}\sqrt{n_1^2-\sin^2\theta}\right)\cdot\frac{2\pi}{c}D\sqrt{n_1^2-\sin^2\theta}\,|_{f=f_0} \quad (21)$$

Substituting it into the formula (7), the E_φ at broadside is expressed by

$$E_\varphi \simeq E_0 \frac{\begin{pmatrix} \sec\left(\frac{2\pi f_0 D}{c}\sqrt{n_1^2-\sin^2\theta_0}\right) \\ +\Delta f \sec^2\left(\frac{2\pi f_0 D}{c}\sqrt{n_1^2-\sin^2\theta_0}\right)\left(\frac{2\pi D}{c}\sqrt{n_1^2-\sin^2\theta_0}\right) \end{pmatrix}}{\begin{pmatrix} 1+j\left[\bar{B}_L+\bar{Y}_1^{TE}\sec\left(\frac{2\pi f_0 D}{c}\sqrt{n_1^2-\sin^2\theta_0}\right)\right. \\ \left. +\bar{Y}_1^{TE}\Delta f\sec^2\left(\frac{2\pi f_0 D}{c}\sqrt{n_1^2-\sin^2\theta_0}\right)\left(\frac{2\pi D}{c}\sqrt{n_1^2-\sin^2\theta_0}\right)\right] \end{pmatrix}} \quad (22)$$

Because the condition of

$$\Delta f \cdot \bar{Y}_1^{TE} \sec^2 \left(\frac{2\pi f_0 D}{c}\sqrt{n_1^2 - \sin^2\theta_0}\right)\left(\frac{2\pi D}{c}\sqrt{n_1^2 - \sin^2\theta_0}\right) = 1 \quad (23)$$

needs to be meet. Substituting formula (7) into (23), the result of pattern bandwidth of E_φ is derived as

$$BW_{3\,\mathrm{dB}} = 2\frac{\Delta f}{f_0} = \frac{4n_1}{\overline{B}_L^2 \pi} \quad (24)$$

For general case, according to the relation ship between the $\Delta\theta$ and Δf, the results of pattern bandwidth of E_φ can be obtained by

$$BW_{3\,\mathrm{dB}} = 2\frac{\Delta f}{f_0} = \frac{4f_0 D}{c}\frac{\sin\theta\cos\theta}{\sqrt{n_1^2 - \sin^2\theta}}\Delta\theta = \frac{4\sqrt{n_1^2 - \sin^2\theta}}{\overline{B}_L^2 \pi \sec\theta} \quad (25)$$

E-Plane: From (8), performing a similar analysis process the explicit expressions of bandwidth in E-plane can be derived as shown in Table 1.

2.3. Radiation Properties of Antenna with PEC Ground

When the ground plane is PEC in Fig. 1(c), the load impedance in the transmission line model is zero. The far field can be determined analogously. The expressions for radiation property such as the field peak values, pattern beamwidth and pattern bandwidth are the same as the results in [9], which are also validated by comparing with numerically exact results obtained from an accurate pattern calculation. The results are also demonstrated in Table 1. The accuracy of these formulas in PEC case indicates that the results in PMC case obtained from TEN model method are creditable in theory, although the existing structures achieve PMC condition that the phase of the reflection lies in some range about zero only at a particular frequency.

2.4. Comparison of Radiation Properties of Antenna with PEC and PMC Ground

Figure 2 shows the far field radiation pattern of E- and H-planes for PMC and PEC ground cases with dielectric substrate permittivity $\varepsilon_{r1} = 2.2$, respectively. Due to the infinite ground, the angle range of θ is limited within $\pm 90^\circ$. In Fig. 2, the peak value of far field in E- and H-planes is the same at broadside direction for two kinds of ground plane. It is obvious that the difference between E-plane and

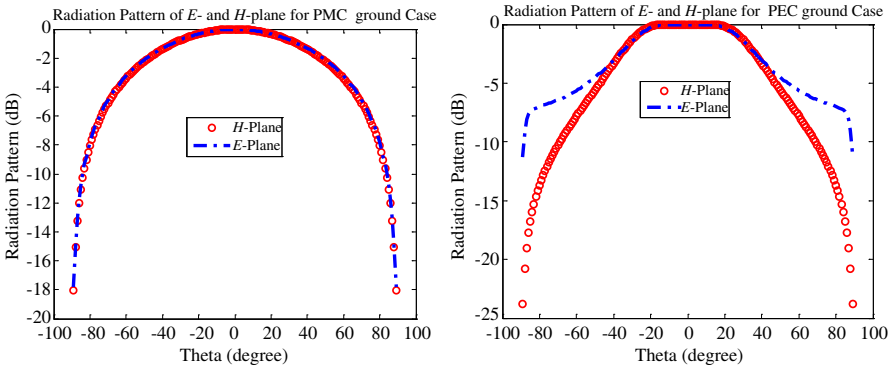

Figure 2. Radiation pattern of E-, H-plane for (a) PMC and (b) PEC cases ($\varepsilon_{r1} = 2.2$, $\bar{B}_L = -2.31$).

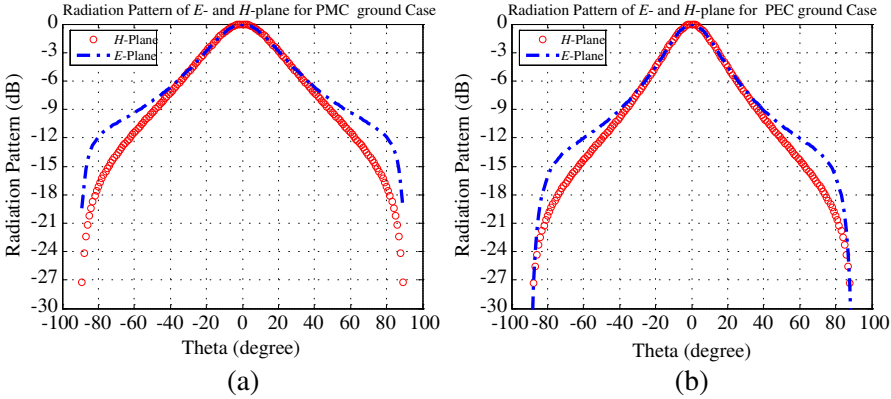

Figure 3. Radiation pattern of E-, H-plane for (a) PMC and (b) PEC cases ($\varepsilon_{r1} = 1$, $\bar{B}_L = -9.14$).

H-plane radiation patterns of PMC case is less than that of PEC case, and the half power beamwidth of PMC case is much large than that of PEC case when dielectric substrate permittivity is larger than 1.

On the other hand, when dielectric substrate permittivity is equal to 1, air is assumed as the medium to fill the parallel-plate region, which is in most case in practical application. And then the normalized admittances $\bar{Y}_1$ for TE and TM polarizations can be simplified as:

$$\bar{Y}_1^{TM} = \eta_0 Y_1^{TM} = \frac{\varepsilon_{r1}}{\sqrt{n_1^2 - \sin^2\theta}} = \frac{1}{\cos\theta} \quad \bar{Y}_1^{TE} = \sqrt{n_1^2 - \sin^2\theta} = \cos\theta \tag{26}$$

Figure 3 shows the far field radiation patterns of E- and H-planes for PMC and PEC ground cases with dielectric substrate permittivity $\varepsilon_{r1} = 1$ and $\bar{B}_L = -9.14$, respectively. In Fig. 3, the fact that the peak value of field in E- and H-planes is the same at broadside direction for two kinds of ground plane is also observed. But the difference between E-plane and H-plane radiation patterns of PMC case is almost the same as that of PEC case.

The comparison result of bandwidth vs. angle for PMC and PEC cases is shown in Fig. 4. It demonstrates that the trends of bandwidth varying with angle in E-plane and H-plane are reverse. The largest bandwidth occurrs in broadside direction in H-plane, while the reverse result is found in E-plane. At broadside direction, the bandwidth of E-plane is equal to that of H-plane. It is obvious that the bandwidth corresponding to the angle for PMC case is twice of that for PEC case in E- and H-planes, although the bandwidths are very narrow.

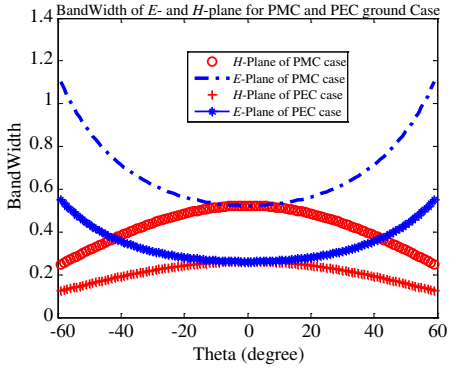

Figure 4. Pattern bandwidth of E-, H-plane for PMC and PEC cases ($\varepsilon_{r1} = 2.2$, $\bar{B}_L = -2.31$).

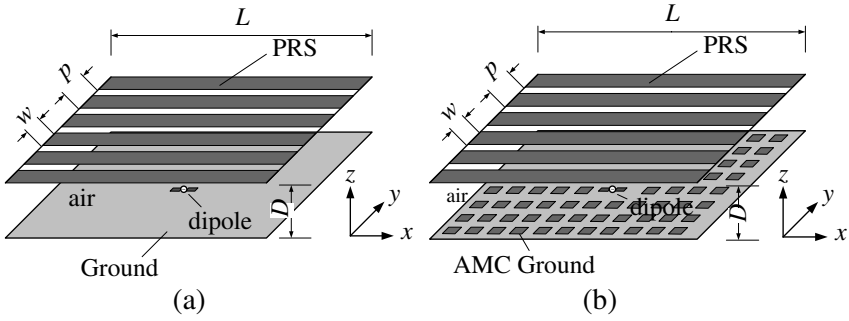

Figure 5. Fabry-Perot Resonator antenna with metal strip as PRS. (a) PEC. (b) AMC case.

3. DISCUSSION

A summary of radiation properties for FPR antenna with PMC or PEC ground plane is shown in Table 1. It is interesting to indicate that the radiation property of FPR antenna with two different ground plane is not always the same.

Firstly, as shown in Table 1, for the same ground plane, either PMC or PEC, at broadside the peak field, the beamwidth and pattern bandwidth in E- and H-planes are identical, whereas at other scan directions, the maximum field, beamwidth and pattern bandwidth in E- and H-planes are not the same. This means that the radiation beam at broadside is symmetrical, which is independent of the type of ground plane. Moreover, radiation beam at other scan directions is nonsymmetrical. It is also indicated that at broadside, the peak fields are equal for all cases. In general scan state, for PMC and PEC the peak field value increases with angle θ in H-plane, while in E-plane, the trend is the opposite. Hence, the larger is the scan angle, the greater is the difference between the peak field values in H- and E-planes.

Secondly, for a different type of ground plane, at broadside the beamwidth in the E- and H-planes of PMC case is the square root of 2 times that of PEC case, whereas at other scan directions the beamwidth in the E- and H-planes of PMC case is 2 times of that of PEC case.

Table 1. Comparative results of radiation property for FPR antenna with two different ground.

		E-Plane	H-Plane
Farfield pattern	PMC	$E_0\cos\theta\frac{\cos k_{z1}h\sec k_{z1}D}{1+j(\bar{B}_L+\bar{Y}_1^{TM}\sec k_{z1}D)\cos\theta}$	$E_0\frac{\cos k_{z1}h\sec k_{z1}D}{1+j(\bar{B}_L+\bar{Y}_1^{TE}\sec k_{z1}D)\sec\theta}$
	PEC	$E_0\cos\theta\frac{\sin k_{z1}h\csc k_{z1}D}{1+j(\bar{B}_L+\bar{Y}_1^{TM}\csc k_{z1}D)\cos\theta}$	$E_0\frac{\sin k_{z1}h\csc k_{z1}D}{1+j(\bar{B}_L+\bar{Y}_1^{TE}\csc k_{z1}D)\sec\theta}$
Peak value (broadside; scan)	PMC	$\frac{E_0\lvert\bar{B}_L\rvert}{n_1}$; $E_0\cos\theta\frac{\lvert\bar{B}_L\rvert\sqrt{n_1^2-\sin^2\theta}}{n_1^2}$	$\frac{E_0\lvert\bar{B}_L\rvert}{n_1}$; $E_0\frac{\lvert\bar{B}_L\rvert}{\sqrt{n_1^2-\sin^2\theta}}$
	PEC	$\frac{E_0\lvert\bar{B}_L\rvert}{n_1}$; $E_0\cos\theta\frac{\lvert\bar{B}_L\rvert\sqrt{n_1^2-\sin^2\theta}}{n_1^2}$	$\frac{E_0\lvert\bar{B}_L\rvert}{n_1}$; $E_0\frac{\lvert\bar{B}_L\rvert}{\sqrt{n_1^2-\sin^2\theta}}$
Beamwidth (broadside; scan)	PMC	$2\sqrt{\frac{4n_1^3}{\bar{B}_L^2\pi}}$; $\frac{4n_1^2\sqrt{n_1^2-\sin^2\theta}}{\bar{B}_L^2\pi\sin\theta\cos^2\theta}$	$2\sqrt{\frac{4n_1^3}{\bar{B}_L^2\pi}}$; $\frac{4(n_1^2-\sin^2\theta)^{3/2}}{\bar{B}_L^2\pi\sin\theta}$
	PEC	$2\sqrt{\frac{2n_1^3}{\bar{B}_L^2\pi}}$; $\frac{2n_1^2\sqrt{n_1^2-\sin^2\theta}}{\bar{B}_L^2\pi\sin\theta\cos^2\theta}$	$2\sqrt{\frac{2n_1^3}{\bar{B}_L^2\pi}}$; $\frac{2(n_1^2-\sin^2\theta)^{3/2}}{\bar{B}_L^2\pi\sin\theta}$
Bandwidth (broadside; scan)	PMC	$\frac{4n_1}{\bar{B}_L^2\pi}$; $\frac{4n_1^2\sec\theta}{\bar{B}_L^2\pi\sqrt{n_1^2-\sin^2\theta}}$	$\frac{4n_1}{\bar{B}_L^2\pi}$; $\frac{4\sqrt{n_1^2-\sin^2\theta}}{\bar{B}_L^2\pi\sec\theta}$
	PEC	$\frac{2n_1}{\bar{B}_L^2\pi}$; $\frac{2n_1^2\sec\theta}{\bar{B}_L^2\pi\sqrt{n_1^2-\sin^2\theta}}$	$\frac{2n_1}{\bar{B}_L^2\pi}$; $\frac{2\sqrt{n_1^2-\sin^2\theta}}{\bar{B}_L^2\pi\sec\theta}$

Thirdly, the bandwidth, including at broadside and at other scan directions, in the E- and H-planes of PMC case is 2 times of that of PEC case. As illustrated in Fig. 4, the trends of bandwidth varying with angle in E-plane and H-plane are reverse for two kinds of ground plane, and at broadside direction the bandwidth of E-plane is equal to that of H-plane.

4. VALIDATION

In order to validate our approach, a simple prototype of antenna with PEC ground plate and air filling, as shown in Fig. 5(a), referred to [2, 29], was simulated by CST Microwave Studio. The height of Fabry-Perot cavity, the distance between two parallel plates, is **D**. A metal strip FSS-type cover constructed by 26 columns strip elements with period $p = 3.0\,\text{mm}$ and size $w = 0.52\,\text{mm}$, $L = 80\,\text{mm}$ is acted as PRS. For the purpose of comparison with TEN model, a x-directed (parallel to the strip axis) electric dipole placed in the middle of cavity ($h = D/2$) is used as the source. The radiation patterns would not be significantly different when using a practical feed such as a slot or a patch antenna inside the cavity.

According to the resonant condition, the height of Fabry-Perot Resonator antenna is determined by [1, 16, 19, 30]

$$D = (\varphi_1 + \varphi_2 - N2\pi)\lambda/4\pi, \quad N = 0, 1, 2\ldots \tag{27}$$

where λ is free space wavelength of operating frequency, and φ_1 and φ_2 are reflection phases of the cover and base, respectively. When **D** is 12.5 mm, the resonant frequency occurs at about 12 GHz. In this situation, an approximate $\bar{B}_L$ can be derived from generalized Sakurai-Vainshtein-Sivov boundary condition [29, 31]

$$\bar{B}_L(k_x, k_0) = \frac{2\pi k_0}{p\left(k_0^2 - k_x^2\right)\ln\csc\left(\frac{\pi w}{2p}\right)} \tag{28}$$

where $k_x = k_0 \sin\theta\cos\varphi$. With indicated values for p and w, the normalized susceptance of PRS is $\bar{B}_L = -9.14$ at resonant frequency 12 GHz. The far field radiation pattern of E- and H-planes of prototype of antenna with PEC is calculated with TEN model by substituting the value of $\bar{B}_L$ into the formula, which is shown in Fig. 3(b). Compared with the results calculated by TEN model, the simulation results of far field radiation pattern at 12 GHz calculated by CST Microwave Studio are shown in Fig. 7(a) and Fig. 8(a). It is indicated that the beamwidth calculated by TEN model agrees well with the one simulated by software.

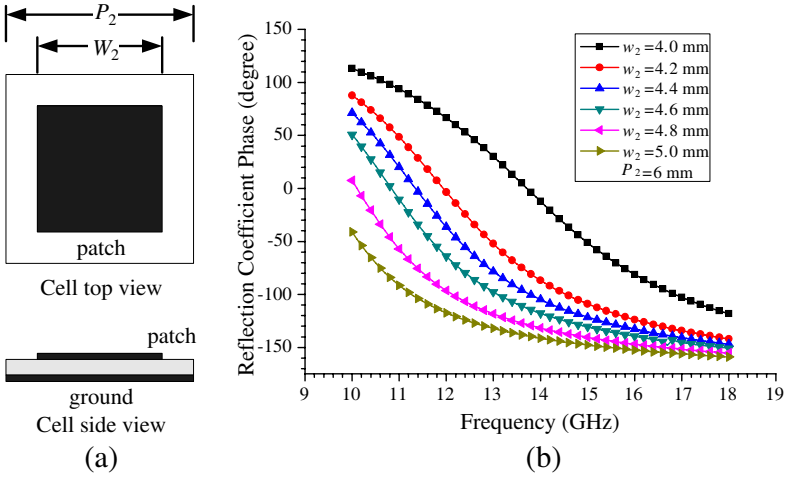

Figure 6. Reflection characteristics of AMC Surface. (a) Periodic cell with square patch. (b) Reflection phase vs. frequency at different patch size.

A prototype of antenna with artificial magnetic conductor (AMC) ground plate [30, 32] is also proposed. The only difference between the prototype of antenna with PEC ground and that with AMC ground is that a 13 rows × 13 columns uniform patch of elements with square-cell (period $p_2 = 6.0\,\text{mm}$) and square-patch (size $w_2 = 4.2\,\text{mm}$) is printed on the upper side of substrate with permittivity 3.2 and thickness 1.57 mm to act as AMC ground plate. In order to perform the parametric study of different patch sizes with the same unit cells, a normally incident plane wave is considered. The reflection phase is then measured while varying the values of different patch sizes. To analyze the AMC behavior, the frequency at which the reflection phase is zero has to be analyzed. Fig. 6 shows the frequency corresponding to reflection phase when varying the patch size. According to the results shown in Fig. 6, with the decrease of the patch size, the in-phase reflection point moves to high frequency, and in-phase reflection behaviour is observed for a frequency value of 12 GHz when the patch size is equal to 4.2 mm. The corresponding optimized **D** is 6.06 mm, then the thickness of antenna is obviously reduced to half. The distance between dipole source and AMC surface is 0.26 mm, which is equivalent to put dipole on the surface of AMC directly.

The far field radiation pattern of E- and H-planes of Fabry-Perot Resonator antenna with PMC ground calculated by TEN method is shown in Fig. 3(a). On the other hand, the simulation results of far field radiation pattern at 11.8 GHz, frequency shift due to the effect

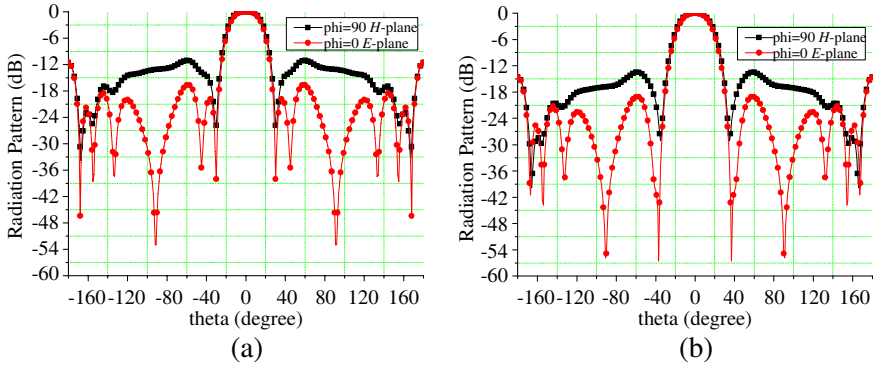

Figure 7. Radiation pattern for two types of ground: (a) PEC and (b) PMC.

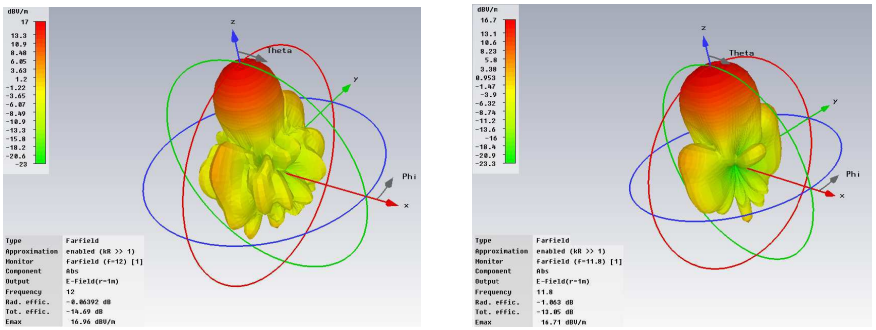

Figure 8. Radiation pattern (3-Dimension) for two types of ground: (a) PEC and (b) PMC.

of source location, calculated by CST Microwave Studio are shown in Fig. 7(b) and Fig. 8(b). It is also illustrated that the beamwidth calculated by TEN model agrees well with that simulated by full wave simulated software.

The peak values of far field for two types of ground at broadside almost all occur at 12 GHz at which the reflection phase is zero for AMC case as shown in Fig. 6. As shown in Fig. 8, the maximum of the field at broadside for PEC case is 16.96 dBV/m, while for AMC case is 16.71 dBV/m, and they are almost the same. It is validated that at broadside the peak fields are equally derived by TEN model for all cases. In addition, it can be observed that, in Fig. 7 and Fig. 8, the beamwidth of AMC case is a little wider than that of PEC case, which is coincident with results also shown in Fig. 3.

5. CONCLUSION

The closed-form expressions for the radiated property of FPR antenna with PMC ground plane are derived from a simple transverse equivalent network model. The comparative results for Fabry-Perot Resonator (FPR) antenna with PMC and PEC ground planes are also presented. An interesting characteristic of this antenna is that in theory the radiation property of FPR antenna with two kinds of ground planes is not the same. Theoretically, the pattern bandwidth of FPR antenna in E- and H-planes with PMC ground is twice as much of that with PEC ground plane. The beamwidth in the E- and H-planes of PMC case is square root of 2 times that of PEC case at broadside, whereas at other scan directions the beamwidth in the E- and H-planes of PMC case is 2 times of that of PEC case. Although in practice the pattern bandwidth of FPR antenna with PMC ground is much less than its theoretical value due to the bandwidth of PMC over which the PMC property can be achieved, which also limits the application of PMC in practice, some original results obtained here is of great significance for antenna designing.

ACKNOWLEDGMENT

This work is supported by a grant (No. 60921063) from National Natural Science Foundation, China.

REFERENCES

1. Trentini, G. V., "Partially reflecting sheet array," *IRE Trans. Antennas Propag.*, Vol. 4, 666–671, 1956.
2. Guerin, N., S. Enoch, G. Tayeb, et al., "A metallic Fabry-Perot directive antenna," *IEEE Trans. Antennas Propag.*, Vol. 54, No. 1, 220–224, 2006.
3. Feresids, A. P., G. Goussetis, S. H. Wang, and J. C. Vardaxoglou, "Artificial magnetic conductor surface and their application to low-profile high-gain planar antennas," *IEEE Trans. Antennas Propag.*, Vol. 53, No. 1, 209–214, 2005.
4. Liu, Z. G., W. X. Zhang, D. L. Fu, et al., "Broadband Fabry-Perot resonator printed antennas using FSS superstrate with dissimilar size," *Microwave & Opt. Tech. Letters*, Vol. 50, No. 6, 1623–1627, 2008.
5. Alexopoulos, N. G. and D. R. Jackson, "Fundamental superstrate

(cover) effects on printed circuit antennas," *IEEE Trans. Antennas Propag.*, Vol. 32, No. 8, 807–816, 1984.

6. Yang, H. Y. and N. G. Alexopoulos, "Gain enhancement methods for printed circuit antennas through multiple superstrates," *IEEE Trans. Antennas Propag.*, Vol. 35, No. 7, 860–863, 1987.
7. Jackson, D. R. and A. Oliner, "A leaky-wave analysis of the high-gain printed antenna configuration," *IEEE Trans. Antennas Propag.*, Vol. 36, No. 7, 905–910, 1988.
8. Jackson, D. R., A. Oliner, and A. Ip, "Leaky wave propagation and radiation for a narrow-beam multiplelayer dielectric structure," *IEEE Trans. Antennas Propag.*, Vol. 41, No. 3, 344–348, 1993.
9. Zhao, T., D. R. Jackson, J. T. Williams, and A. A. Oliner, "General formulas for 2D leaky-wave antennas," *IEEE Trans. Antennas Propag.*, Vol. 53, No. 11, 3525–3533, 2005.
10. Costa, F. and A. Monorchio, "Design of subwavelength tunable and steerable Fabry-Perot/leaky wave antennas," *Progress In Electromagnetics Research*, Vol. 111, 467–481, 2011.
11. Thevenot, M., C. Cheype, A. Reineix, and B. Jecko, "Directive photonic-bandgap antennas," *IEEE Trans. Antennas Propag.*, Vol. 47, No. 11, 2115–2122, 1999.
12. Cheype, C., C. Serier, M. Thèvenot, et al., "An electromagnetic bandgap resonator antenna," *IEEE Trans. Antennas Propag.*, Vol. 50, No. 9, 1285–1290, 2002.
13. Lee, Y. J., J. Yeo, R. Mittra, and W. S. Park, "Design of a high-directivity electromagnetic band gap resonator antenna using a frequency-selective surface superstrate," *Microwave & Opt. Tech. Lett.*, Vol. 43, No. 6, 462–467, 2004.
14. Weily, A. R., L. Horvath, K. P. Esselle, et al., "A planar resonator antenna based on a woodpile EBG material," *IEEE Trans. Antennas Propag.*, Vol. 53, No. 1, 216–223, 2005.
15. Pirhadi, A. and M. Hakkak, "Design of compact dual band high directive electromagnetic bandgap (EBG) resonator antenna using artificial magnetic conductor," *IEEE Trans. Antennas Propag.*, Vol. 55, No. 6, 1682–1690, 2007.
16. Ge, Y. and K. P. Esselle, "A method to design dual-band, high-directivity EBG resonator antennas using single-resonant, single-layer partially reflective surfaces," *Progress In Electromagnetics Research C*, Vol. 13, 245–257, 2010.
17. Boutayeb, H., K. Mahdjoubi, A. C. Tarot, et al., "Directivity of an antenna embedded inside a Fabry-Perot cavity analysis and design," *Microwave & Opt. Tech. Lett.*, Vol. 48, No. 1, 12–17,

2006.

18. Boutayeb, H., T. A. Denidni, and M. Nedil, "Bandwidth widening techniques for directive antennas based on partially reflecting surfaces," *Progress In Electromagnetics Research*, Vol. 74, 407–419, 2007.
19. Liu, Z. G., "Fabry-Perot resonator antenna," *Journal of Infrared Milli Terahz Waves*, Vol. 31, No. 4, 391–403, 2010.
20. Liu, Z. G. and R. Qiang, "A novel broadband Fabry-Perot resonator antenna with gradient index metamaterial superstrate," *IEEE International Symposium on Antennas and Propag.*, Toronto, Canada, Jul. 11–17, 2010.
21. Liu, Z. G., "Research progress on Fabry-Perot resonator antenna," *Journal of Zhejiang University SCIENCE A*, Vol. 10, No. 4, 583–588, 2009.
22. Sievenpiper, D., "High-impedance electromagnetic surfaces," Ph.D. Dissertation, Dept. Elect. Eng., Univ. California at Los Angeles, 1999.
23. Sievenpiper, D., L. Zhang, R. Broas, N. Alexopolous, and E. Yablonovitch, "High-impedance frequency selective surfaces with a forbidden frequency band," *IEEE Trans. Microwave Theory Tech.*, Vol. 47, No. 11, 2059–2074, 1999.
24. Yang, F., K. Ma, Y. Qian, and T. Itoh, "A uniplanar compact photonic-bandgap (UC-PBG) structure and its applications for microwave circuits," *IEEE Trans. Microwave Theory Tech.*, Vol. 47, No. 8, 1509–1514, 1999.
25. Pirhadi, A., M. Hakkak, and F. Keshmiri, "Using electromagnetic bandgap superstrate to enhance the bandwidth of probe-fed microstrip antenna," *Progress In Electromagnetics Research*, Vol. 61, 215–230, 2006.
26. Pirhadi, A., F. Keshmiri, M. Hakkak, and M. Tayarani, "Analysis and design of dual band high directive EBG resonator antenna using square loop FSS as superstrate layer," *Progress In Electromagnetics Research*, Vol. 70, 1–20, 2007.
27. Foroozesh, A., M. N. M. Kehn, and L. Shafai, "Application of artificial ground planes in dual-band orthogonally-polarized low-profile high-gain planar antenna design," *Progress In Electromagnetics Research*, Vol. 84, 407–436, 2008.
28. Liu, Z. G. and R. Qiang, "Comparative approach of Fabry-Perot resonator antenna with PMC and PEC ground plane," *IEEE International Symposium on Antennas and Propag.*, Toronto, Canada, Jul. 11–17, 2010.

29. Burghignoli, P., G. Lovat, F. Capolino, and D. R. Jackson, "Highly polarized directive radiation from a Fabry-Perot cavity leaky-wave antenna based on a metal strip grating," *IEEE Trans. Antennas Propag.*, Vol. 58, No. 12, 3873–3883, 2010.
30. Feresidis, A. P. and J. C. Vardaxoglou, "High gain planar antenna using optimised partially reflective surfaces," *IEE Proc. Microw. Antennas Propag.*, Vol. 148, No. 6, 345–350, 2001.
31. Kaganovsky, Y. and R. Shavit, "Analysis of radiation from a line source in a grounded dielectric slab covered by a metal strip grating," *IEEE Trans. Antennas Propag.*, Vol. 57, No. 1, 135–143, 2009.
32. Yousefi, L., H. Attia, and O. M. Ramahi, "Broadband experimental characterization of artificial magnetic materials based on a microstrip line method," *Progress In Electromagnetics Research*, Vol. 90, 1–13, 2009.